HHS Public Access

Author manuscript

J Am Chem Soc. Author manuscript; available in PMC 2017 November 09.

Published in final edited form as:

J Am Chem Soc. 2016 November 09; 138(44): 14616–14622. doi:10.1021/jacs.6b06820.

The N-terminal amphipathic helix of Endophilin does not contribute to its molecular curvature generation capacity

Zhiming Chen[1], **Chen Zhu**[1], **Curtis J. Kuo**[1], **Jaclyn Robustelli**[1], and **Tobias Baumgart**[1,*]

[1]Department of Chemistry, University of Pennsylvania, Philadelphia, USA

Abstract

N-BAR proteins such as endophilin are thought to bend lipid membranes via scaffolding (the molding of membranes through the crescent protein shape) and membrane insertion (also called wedging) of amphipathic helices. However, the contributions from these distinct mechanisms to membrane curvature generation and sensing have remained controversial. Here we quantitatively demonstrate that the amphipathic N-terminal H0 helix of endophilin is important for recruiting this protein to the membrane, but does not contribute significantly to its intrinsic membrane curvature generation capacity. These observations elevate the importance of the scaffolding mechanism, rather than H0 insertion, for the membrane curvature generation by N-BAR domains. Furthermore, consistent with the thermodynamically required coupling between curvature generation and sensing, we observed that the H0-truncated N-BAR domain is capable of sensing membrane curvature. Overall, our contribution clarifies an important mechanistic controversy in the function of N-BAR domain proteins.

TOC image

Corresponding Author: Tobias Baumgart: baumgart@sas.upenn.edu.

Supporting Information Placeholder

Notes

The authors declare no competing financial interests.

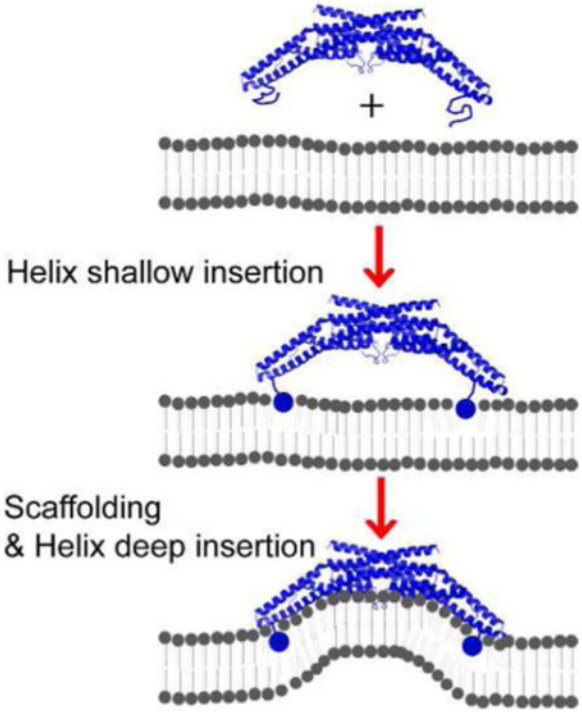

Introduction

The shape diversity of cell membranes is regulated in part by the large family of BAR (Bin/Amphiphysin/Rvs) domain containing proteins[1]. Endophilin belongs to the class of N-BAR proteins. Members of this type contain an N-terminal helix (also named H0) that amphipathically inserts into the membrane as well as a BAR domain that can homo-dimerize to form a crescent-shaped structure. This BAR domain dimer is thought to act as a scaffold to enable membrane curvature remodeling[2]. In this contribution, we use the term "scaffolding" to describe the molding of the membrane through the crescent shape of the protein in general and the concave membrane-binding interface in particular. The role of H0 helix insertion versus the BAR dimer scaffolding mechanism in membrane curvature generation and sensing has remained controversial.

Several reports have argued that both H0 amphipathic insertion and BAR dimer scaffolding can drive membrane bending[2–7] and that H0 insertion promotes membrane scission[6,7], although the latter has recently been questioned[8]. Steric repulsion arising from protein-protein crowding has also been considered as a driving force for membrane curvature generation[9]. This mechanism is general and would be effective for any peripheral membrane protein if present at sufficiently high density. However, we have shown that N-BAR domains such as endophilin induce membrane curvature changes at low protein coverage where the crowding effect is negligible[10].

Based on continuum mechanical models[11], molecular dynamics (MD) simulations[12], and experimental evidence[13], H0 amphipathic insertion has been described as solely sufficient to generate membrane curvature if H0 helices are present at a high enough membrane surface

density. On the other hand, MD simulation studies from Cui et al.[14] and Blood et al.[15] suggest that amphipathic helix folding through membrane interaction of N-BAR domains either requires the membrane to be already bent, or requires the amphipathic helices to be more concentrated than physiological conditions to induce curvature. Furthermore, results from Blood et al.[15] imply that the close association of the charged concave surface of the N-BAR domain is required for its membrane curvature induction and that membrane curvature is not driven by the membrane-embedded amphipathic helices. However, amphipathic helices were shown to be essential to maintain close association of the concave surface of the N-BAR domain with the membrane[15,16]. Consistent with this notion, MD simulations from Arkhipov et al.[17], later refined by Lyman et al.[18], also suggested that BAR dimer scaffolding, rather than helix insertion, is the key player in membrane bending by N-BAR domains. That said, MD simulations typically investigate local membrane curvature generation in the neighborhood of either a single, or a small number, of BAR proteins whereas experimental studies such as those presented here assess global curvature generation in terms of budding and tubulation events. This fact, and the coarse graining underlying most MD simulations of curvature sensitive proteins, challenges the comparison between experimental and simulated phenomena. However, experimental reports exist that are consistent with the notion that the H0 helix is not essential for membrane curvature generation through N-BAR domains[19], and that the H0 peptide alone cannot alter liposome morphology[20].

In membrane curvature sensing, Bhatia et al. reported that amphipathic motifs are essential for the membrane curvature sensing of BAR domains[21,22], based on sensing local, curvature-dependent membrane bilayer defects[23,24]. On the other hand, the asset of the dimeric BAR domain structure in favoring the geometry of curved membrane was also discussed by Doucet et al.[25], emphasizing a possible role of the BAR domain scaffold in membrane curvature sensing.

Clearly, the role of the H0 helix in both curvature generation and sensing requires clarification. In this contribution, we designed mutants and used *in vitro* biophysical tools to specifically study the contributions of amphipathic helix insertion to endophilin N-BAR domain membrane binding, curvature generation capacities, and membrane curvature sensing. We revealed that the amphipathic helix dominates the membrane binding of endophilin N-BAR, which influences the overall tubulation capacity of endophilin N-BAR. However, our results also show that amphipathic insertion does not contribute to the molecular curvature generation ability of endophilin N-BAR. Finally, we revealed that the endophilin BAR domain (without H0 helix) is capable of sensing membrane curvature, while the H0 helix contributes to the nonlinear curvature sorting of endophilin N-BAR.

Results and Discussion

To distinguish the role of H0 hydrophobic insertion and BAR dimer scaffolding, we designed endophilin N-BAR variants with varied H0 properties (hydrophobicity, length) to specifically study the contribution from H0 insertion.

As shown in Figure 1A, the endophilin N-BAR domain was modified either by single-site mutagenesis or truncation. Residue F10 is the most hydrophobic residue (Fig. 1B–C) within the H0 wild-type (WT) domain and was reported to insert into the membrane[2]. We thus mutated this residue to either one with greater hydrophobicity (F10W) to enhance H0 membrane insertion or with a small residue (F10A) to reduce H0 insertion. In addition to single site mutagenesis, we progressively truncated the H0 helix to investigate the effect of H0 length. Circular dichroism proved that the mutations did not affect the helicity of the protein (Fig. 1D) for any of the variants.

To delineate the role of the H0 helix in endophilin function, we first compared the membrane binding capacity of the endophilin variants. Our results show that the F10W mutant binds to the membrane stronger than the WT protein under the same bulk concentration, while the F10A mutant binds significantly weaker (Fig. 2A). This observation is expected due to the different side chain hydrophobicities. The binding capacity of the truncation variants under the same bulk concentration decreased with decreasing length of the H0 helix (Fig. 2A, equilibrium density: WT > D1-6 > D1-10 > D1-14 > D1-18 > D1-24). These observations indicate that the H0 helix plays a key role in the binding of endophilin N-BAR to the membrane[29].

The linear relationship (Fig. 2B) between logarithmic densities and helix length is consistent with a roughly linear dependence of the free energy of binding on helix length. However, the membrane binding density of the H0 total deletion variant (D1-24) showed no significant difference from that of the D1-18 variant, which likely implies that residues 19–24 do not significantly contribute to membrane binding. The absence of a discernible contribution to membrane binding from residues 19–24 suggests that this region does not significantly interact with the membrane, consistent with the predicted absence of helical structure in this region (Fig. 1B). Furthermore, the basal degree of membrane binding of the D1-24 truncate implies that H0 interaction with the membrane is the dominant, but not the only contributor, to endophilin N-BAR's membrane binding. Other mechanisms such as 1) H1 insert helix (H1i, residues: 59–87) membrane binding and 2) electrostatic interactions between the positively charged concave dimer surface and the negatively charged membrane, could contribute to attract the protein to the membrane. Indeed, the S75D (within H1i) mutant showed reduced membrane binding (Fig. 2A), as expected[30].

We next compared the intrinsic membrane curvature generation capacities of the variants to WT protein. A giant unilamellar vesicle (GUV) shape stability assay[31,32] served to quantify the protein density required to induce membrane curvature changes on membrane tension-controlled GUVs. In this assay, a single vesicle was aspirated from a GUV dispersion, set under a specific membrane tension (Fig. 3A, see Materials and Methods for calculation of tension, σ), and then transferred to a protein solution, followed by confocal imaging to monitor the protein density on the GUV as well as GUV geometry changes (Fig. 3B). Fig. 3B shows that when N-BAR domain binding reached a threshold density level, the projection length inside the glass pipette began to decrease and tubules formed towards the GUV exterior (Fig. 3B, red arrow, note that individual tubules are not resolved but result in fluorescent blur near the vesicle[31,32]). The point where the apparent area, $Area(t)=4\pi R_v^2(t)+2\pi R_P L_P(t)$, of the GUV starts to decrease (red arrow indicates the

transition point in Fig. 3C) corresponds to a membrane-curvature-instability-transition protein density (Fig. 3C), which combined with the selected membrane tension is an indicator of the intrinsic membrane curvature generation capacity of the protein (see Materials and Methods for details)[32]. Note that transition densities of the three shortest variants could not be determined because their low membrane binding capacity required bulk solution concentrations high enough to cause background fluorescence intensities that interfered with the measurement of fluorescence levels at the membrane.

In sharp contrast to the significant contribution of the H0 helix to membrane binding, the endophilin variants with either enhanced or inhibited membrane binding capacity showed no significant difference in the transition density at the same membrane tension (Fig. 3D), suggesting that all variants use the same mechanism to initiate bending of membranes.

We observed through classical negative stain transmission electron microscopy (TEM) imaging of membrane tubulation that variants with inhibited membrane binding are less efficient in liposome tubulation. This assay provides the most commonly used readout for membrane curvature generation (Fig. 4). This apparent discrepancy with the findings shown in Fig. 3 is easily explained by distinguishing between the intrinsic molecular capacity of a membrane bound protein to generate curvature (assessed in Fig. 3D), and the efficiency with which a bulk solution can tubulate vesicles (assessed via classical TEM based tubulation assays). Only the latter is affected by the membrane binding capacity of the protein of interest. This conclusion is confirmed by the observation that the logarithmic tubulation efficiency (Fig. 4C) follows an essentially linear relationship (slope in Fig. 4C is close to 1) with the logarithm of equilibrium density on the membrane (Fig. 2), implying that the overall tubulation efficiency of an endophilin N-BAR solution is linearly correlated with the membrane binding capacity of the protein.

Taken together, our findings so far are consistent with the notion that the amphipathic insertion of the H0 helix is not responsible for membrane bending through N-BAR domains. To exclude the possibility that H1i, rather than H0, engages in amphipathic wedging through endophilin[33], we examined the H1i mutant S75D. This mutation has previously been shown to reduce the membrane insertion of the H1i helix[30]. As shown in Fig. 3D, this effect does not affect endophilin’s curvature generation capacity.

Our present and previous[32] findings of endophilin function are all consistent with a recent characterization of endophilin membrane association, H0 insertion, and membrane deformation[34]. However, our current analysis implies that the process of endophilin H0 membrane insertion, which was observed to coincide with membrane deformation[34], is a consequence, rather than a cause, of membrane deformation through endophilin. This implication is supported by a previous simulation report showing that H0 folding and insertion is much less energetically favorable in flat membranes, but that it is facilitated in curved membranes with packing defects[14].

To understand the role of the H0 helix in sensing membrane curvature, we compared the membrane curvature sorting of endophilin WT and its H0 deletion mutant with a GUV-pulled tether system (see Materials and Methods for details regarding this method)[35].

In contrast to the known non-linear sorting of endophilin WT N-BAR domains[35], we observed (Fig. 5) that the H0 deletion variant followed linear sorting with membrane curvature (higher membrane tension corresponds to higher membrane curvature on the pulled tether), indicating that the BAR domain without H0 insertion is capable of sensing membrane curvature. This observations is consistent with previous reports showing that F-BAR[36] and I-BAR[37] domains lacking in terminal amphipathic helices also sort on membrane tubules.

In the range of relatively low membrane curvature ($1/R_t < 0.03$ nm^{-1}), the curvature sorting of the H0 deletion variant is comparable to WT protein (Fig. 5B). However, when membrane curvature further increases ($1/R_t > 0.03$ nm^{-1}), the curvature sorting of the H0 deletion variant was observed to be significantly weaker than WT protein (Fig. 5). This observation can be rationalized by the fact that 1) higher membrane curvature creates more membrane bilayer defects and 2) amphipathic motifs (such as H0 helix in endophilin) sense such curvature-dependent membrane bilayer defects[21–24].

Taken together, these results imply that curvature sorting of the N-BAR domain is driven by both the H0 helix (which may contribute to non-linear sorting of endophilin[35]), and by the BAR domain.

The role of H0 densities on the membrane

Our observation that amphipathic H0 helix insertion/wedging does not contribute to curvature generation is not consistent with earlier suggestions that the H0 helix of the N-BAR domain might be solely responsible for generating membrane curvature. This discrepancy can be re-solved by considering the fractional coverage of H0 helices on membranes. MD simulations from Blood et al. indicated that the H0 helix of the N-BAR domain cannot bend the membrane at an H0 density of 150 lipids/embedded helix (corresponding to ~ 5.7% protein coverage assuming helix cross sectional area = 6 nm^2 and area per lipid = 0.7 nm^2). Furthermore, they showed that membranes can only be bent through H0 helices at 30 lipids/embedded helix, an unrealistically high density which would be equivalent to ~ 28.5% helix coverage on the membrane[15]. Consistent with these results, MD simulations from Arkhipov et al. also showed that at 12.5 –18.8% coverage fraction, the amphiphysin H0 cannot induce membrane curvature. These authors further noted that the high H0 density of ~ 30% would compromise the ability of N-BAR domains to bend the membrane because the scaffolding effect of the BAR dimers would be inhibited[38]. The membrane-curvature-instability-transition protein densities shown in Figure 3D are around ~ 2000/μm^2, corresponding to < 2% H0 coverage, i.e. a range where MD simulations have predicted absence of curvature generation through H0 alone.

Furthermore, the endophilin density of ~ 2000/μm^2 corresponds to an overall protein coverage of ~ 6.7%, which is smaller than the coverage fractions cited by Stachowiak et al., where 20 – 30% coverage was shown to be required to bend membranes through crowding at negligible tension (i.e. no pipette aspiration)[9]. Our previous membrane tension-controlled studies also demonstrated that at this relatively low protein coverage (~ 6.7%), the crowding effect is negligible for the membrane curvature generation of endophilin[10].

The role of membrane binding capacity

The previous reports arguing that H0 amphipathic insertion drives membrane curvature could be due to the missing distinction between the role of the H0 helix in associating N-BAR proteins to the membrane versus its capacity to generate membrane curvature. Previous contributions hypothesized that H0 insertion is essential for membrane curvature generation based on the observation that N-BAR variants with compromised H0 insertion showed lower liposome tubulation efficiencies[2,7]. Our findings explain this observation through the reduced membrane binding capacity of H0 truncated mutants. Consistent with this notion, Peter et al.'s liposome tubulation assay to assess the tubulating activity of wild-type N-BAR potentially explains the discrepancy between the controversial observations: buds on liposomes, tubules, and small vesicles were increasingly observed with higher protein concentrations[19]. This notion is further supported by Blood et al.'s MD simulation studies, where H0 insertion played a key role to ensure close association of the charged concave surface of N-BAR domain to membrane and thus drive membrane curvature. Without amphipathic helix insertion, N-BAR domain's membrane binding was compromised and failed to drive membrane curvature[15,16]. Taken together, this implies that only studies that determine the density of proteins on the membrane can assess the intrinsic, molecular curvature generation capacity of a membrane binding protein.

The role of lattice formation

The H0 helix was reported to mediate the formation of stable endophilin N-BAR lattices on the membrane[39,40], which was hypothesized to be important for its membrane curvature generation[39]. However, we observed that the D1-10 mutant, which was reported to show a higher degree of lattice disorder compared with the WT protein[39], showed uncompromised membrane curvature induction capacity (Fig. 3D). This observation is consistent with a report for the N-BAR protein BIN1 showing that a low long-range order N-BAR coat was capable of inducing flexible membrane tubules[41]. Taken together, these observations are consistent with the notion that formation of highly ordered stable lattices is not essential for the curvature generation of N-BAR proteins.

The implication of curvature sorting in Clathrin-mediated endocytosis

The diameter of a clathrin-coated vesicle ranges from 70 nm to 150 nm[42], which corresponds to the region $1/R_t < 0.03\ nm^{-1}$ in Fig. 5B. In this region, we find that both endophilin WT and D1-32 show vanishingly small sensitivity to membrane curvature changes. On the other hand, the neck area (diameter: 25 nm – 30 nm[43]) of the clathrin-coated pit is more highly curved and corresponds to the region $1/Rt > 0.06\ nm^{-1}$, where the WT shows strong membrane curvature sorting while the H0 deletion mutant's membrane curvature sorting is much weaker compared to the WT. This observation firstly explains why endophilin is recruited to the neck area of the clathrin-coated pit. Secondly, although the H0 deletion variant is still capable of sensing membrane curvature, its capacity is relatively weak and potentially compromises the specific recruitment of endophilin to the neck area, implying that the H0 helix is essential for endophilin's physiological function in clathrin-mediated endocytosis.

Conclusion

In summary, we have quantitatively studied the membrane binding, curvature generation, and curvature sorting of endophilin N-BAR and its variants with modified H0 amphipathic insertion abilities. We revealed that, for N-BAR domains, the H0 helix plays a key role in membrane binding, but does not influence the protein density required to initiate a membrane curvature transition. Our observations demonstrate that the H0 amphipathic insertion/wedging mechanism of the N-BAR domain of endophilin does not directly induce membrane curvature; instead, other mechanisms, such as BAR dimer scaffolding, appear to be more important for membrane curvature generation. Furthermore, we revealed that the H0 truncated variant was capable of sensing membrane curvature, indicating that sensing as well does not exclusively depend on H0. Overall, this contribution shed light on the controversial state of the biophysical mechanism of endophilin function.

Materials and Methods

Protein preparation

A plasmid encoding GST-tagged endophilin N-BAR domain with mutations C108S and E241C for minimally perturbing fluorescence labeling, noted as WT in this manuscript, was generated as described in reference[44]. This plasmid was further used to generate mutants: 1) single site mutagenesis: F10W, F10A and S75D; 2) truncation mutagenesis: deletion of N-terminal residues 1-X (D1-6, D1-10, D1-14, D1-18, D1-24 and D1-32). The fusion proteins were expressed in BL21(DE3) RIL CodonPlus bacteria (Stratagene, La Jolla, CA). After cell lysis, the supernatant was first applied to a GSTrap FF affinity column (GE Healthcare, Marlborough, MA), and the eluted fusion proteins were cleaved with PreScission Protease[44]. After cleavage, the target protein contains a 5 residue tail (GlyProLeuGlySer) at the N-terminus corresponding to BamH I restriction site and protease cutting site, which is predicted to not form secondary structure[27]. The digestion product was then subjected to a HiTrap Q HP column (GE Healthcare, Marlborough, MA) and a HiLoad Superdex 200 PG column (GE Healthcare, Marlborough, MA)[44]. All proteins were labeled with Alexa Fluor® 488 C5 Maleimide (Thermo Fisher Scientific, Philadelphia, PA) at residue C241 and excess dye was removed by HiTrap Desalting columns (GE Healthcare, Marlborough, MA). Proteins were stored in buffer containing 20 mM HEPES, 150 mM NaCl, and 1 mM TCEP at pH = 7.4. HEPES (4-(2-hydroxyethyl)-1-piperazineethanesulfonic acid) was obtained from SIGMA-ALDRICH® (Allentown, PA), NaCl (sodium chloride) was obtained from Thermo Fisher Scientific (Philadelphia, PA), and TCEP-HCl (tris (2-carboxyethyl) phosphine hydrochloride) was obtained from Pierce/Thermo Fisher Scientific (Rockford, IL). Note that the protein concentrations indicated in this manuscript refer to monomer concentrations, while the protein densities on the membrane refer to homodimer densities.

Liposome preparation

Lipids DOPC (1,2-dioleoyl-sn-glycero-3-phosphocholine), DOPS (1,2-dioleoyl-sn-glycero-3-phospho-L-serine), DOPE (1,2-dioleoyl-sn-glycero-3-phosphoethanolamine), and DSPE-Bio-PEG2000 (distearoylphosphatidylethanolamine – N - (biotinyl (polyethylene glycol) 2000)) were obtained from Avanti Polar Lipids (Alabaster, AL). Texas Red® DHPE

(Texas Red® 1,2-Dihexadecanoyl-sn-Glycero-3-Phosphoethanolamine, Triethylammonium Salt) was obtained from Invitrogen/Life Technologies (Grand Island, NY).

For preparation of large unilamellar vesicles (LUVs)[45], a lipid mixture containing 45% DOPS, 30% DOPE and 25% DOPC was first dried with compressed air and then desiccated at least 2 hours before rehydration. The protein storage buffer was used to rehydrate lipids at a concentration of 1 mg/ml. Rehydrated lipids were vortexed occasionally at room temperature for 1 hour. Next, the dispersions were extruded 13 times through a single polycarbonate membrane of 400 nm pore size (Whatman/GE Healthcare). The resulting LUVs were stored at 4°C and used within two days.

Giant unilamellar vesicles (GUVs) containing 1) 45%DOPS, 30%DOPE, 24.5%DOPC and 0.5% TexasRed DHPE and 2) 64%DOPC, 25%DOPG, 10% PI(4,5)P2, 0.3% TexasRed DHPE and 0.7% DSPE-Bio-PEG2000 were electroformed in 300 mM sucrose as described in refs[31,32,45,46].

Liposome tubulation assay

0.1 mg/ml LUVs were co-incubated with 10 μM protein solution for 30 min and then put on TEM grids (Formvar/Carbon 200 mesh, Copper grids, Electron Microscopy Sciences, Hatfield, PA) for 2 min. Before negative staining with 2% (w/v) uranyl acetate, the grids were first rinsed in buffer and blotted with filter paper to remove excess materials. After staining, the grids were dried gently and then imaged with a JEM 1011 transmission electron microscope (JEOL).

GUV shape stability assay

The GUV shape stability assay was carried out as described in ref[31,32]. As illustrated in Figure 2A, a GUV with controlled membrane tension[46],

$$\sigma=\frac{\Delta P}{2(\frac{1}{R_p}-\frac{1}{R_v})},$$

was aspirated and transferred from a GUV dispersion to a protein solution. During the transfer, the glass pipette used for GUV aspiration was casein-coated to reduce attachment of protein/lipid membrane to the glass pipette[47], and the GUV was protected from dehydration with an outer capillary[44]. The transfer is followed by confocal imaging (Objective: 60× W 1.1 NA, Olympus, Center Valley, PA) to monitor the protein binding and GUV shape changes. The apparent area of the GUV was defined to be:

$$Area(t)=4\pi R_v^2(t)+2\pi R_p L_p(t),$$

which was used as an indicator of the GUV membrane curvature changes since tubulation or vesiculation from the GUV causes a change in the apparent area of the GUV. When protein density reached a GUV-shape-instability transition point, the apparent area started to decrease. This transition density, combined with the chosen membrane tension, is an

indicator of the intrinsic membrane curvature generation ability of the protein[31,32]. The GUV-shape instability transition threshold was rigorously defined as described in ref[31]. Briefly, the standard deviation (SD) and the average value of the apparent area of pre-transition points were calculated and the threshold was determined by subtracting 2X SD from the average value, where the corresponding transition protein density was extracted.

In this assay, the GUV dispersion and protein solutions were prepared by diluting from concentrated stocks with buffer containing 400 mM sucrose, 400 mM glucose, and protein buffer with a ratio of 1:1:1. All measurements were done at room temperature.

The fluorescence intensity obtained from imaging was converted to protein density on the membrane using a calibration with standard BODIPY labeled lipids, where the brightness difference between BODIPY and Alexa 488 dyes was taken into account[31,32,48].

Curvature sorting assay

As described in refs[35,49], a GUV-pulled tether system was used to test the membrane curvature sorting of proteins. Briefly, GUV dispersions were co-incubated with proteins to reach binding equilibrium, then streptavidin-coated polystyrene beads were added to the mixture, and the whole solution was placed in a glass chamber and mounted onto a confocal microscope. Two micropipettes were inserted into the chamber: one to aspirate a GUV, and the other one to aspirate a streptavidin-coated bead, attached to the membrane via biotin-streptavidin coupling, to pull a cylindrical tether from the GUV with ~ 20 μm in length. The membrane tension on the pulled-tether-GUV system was controlled by adjusting the height of a water reservoir, and aspiration pressures were detected with a differential pressure transducer (Validyne Engineering, Los Angeles, CA). The radius of the pulled-tube was calculated from membrane tension based on the model used in Ref.[48]. The fluorescence intensities of labeled protein (Alexa 488) and lipid (Texas Red DHPE) on the tether were recorded through xz scans of the cross-section of the tether (with a stepwidth of 0.07 μm and a total imaging depth of 6 μm) under varied membrane tension, and the ratio ($I_r=I_{green}/I_{red}$) was normalized by the ratio on the vesicle ($I_r^0=I_{ves\text{-}green}/I_{ves\text{-}red}$). The aspiration pressure was changed to obtain I_r/I_r^0 as a function of tube radius on a pulled-tether. For each pulling step, the images were taken at least 90 s after pressure change at constant tether length to make sure the lateral tension reached equilibrium. Buffers used for these measurements were the same as those used in the GUV shape stability assay.

Supplementary Material

Refer to Web version on PubMed Central for supplementary material.

Acknowledgments

We thank the National Institutes of Health (grant No. GM 097552) for financial support, and Zachary Graber and Samantha Wilner for helpful comments on the manuscript.

References

1. Simunovic M, Voth GA, Callan-Jones A, Bassereau P. Trends Cell Biol. 2015; 25:780. [PubMed: 26519988]

2. Gallop JL, Jao CC, Kent HM, Butler PJG, Evans PR, Langen R, T McMahon H. EMBO J. 2006; 25:2898. [PubMed: 16763559]
3. Masuda M, Mochizuki N. Semin Cell Dev Biol. 2010; 21:391. [PubMed: 20083215]
4. Qualmann B, Koch D, Kessels MM. EMBO J. 2011; 30:3501. [PubMed: 21878992]
5. Drin G, Antonny B. FEBS Lett. 2010; 584:1840. [PubMed: 19837069]
6. Boucrot E, Pick A, Camdere G, Liska N, Evergren E, McMahon HT, Kozlov MM. Cell. 2012; 149:124. [PubMed: 22464325]
7. Adam J, Basnet N, Mizuno N. Sci Rep-UK. 2015; 5:15452.
8. Renard H-F, Simunovic M, Lemiere J, Boucrot E, Garcia-Castillo MD, Arumugam S, Chambon V, Lamaze C, Wunder C, Kenworthy AK, Schmidt AA, McMahon HT, Sykes C, Bassereau P, Johannes L. Nature. 2015; 517:493. [PubMed: 25517096]
9. Stachowiak JC, Schmid EM, Ryan CJ, Ann HS, Sasaki DY, Sherman MB, Geissler PL, Fletcher DA, Hayden CC. Nat Cell Biol. 2012; 14:944. [PubMed: 22902598]
10. Chen Z, Atefi E, Baumgart T. Biophys J. 2016; 111
11. Campelo F, McMahon HT, Kozlov MM. Biophys J. 2008; 95:2325. [PubMed: 18515373]
12. Sodt, Alexander J., Pastor, Richard W. Biophys J. 2014; 106:1958. [PubMed: 24806928]
13. Löw C, Weininger U, Lee H, Schweimer K, Neundorf I, Beck-Sickinger AG, Pastor RW, Balbach J. Biophys J. 2008; 95:4315. [PubMed: 18658220]
14. Cui H, Lyman E, Voth GA. Biophys J. 2011; 100:1271. [PubMed: 21354400]
15. Blood PD, Swenson RD, Voth GA. Biophys J. 2008; 95:1866. [PubMed: 18469070]
16. Blood PD, Voth GA. Proc Natl Acad Sci U S A. 2006; 103:15068. [PubMed: 17008407]
17. Arkhipov A, Yin Y, Schulten K. Biophys J. 2009; 97:2727. [PubMed: 19917226]
18. Lyman E, Cui HS, Voth GA. Biophys J. 2010; 99:1783. [PubMed: 20858422]
19. Peter BJ, Kent HM, Mills IG, Vallis Y, Butler PJG, Evans PR, McMahon HT. Science. 2004; 303:495. [PubMed: 14645856]
20. Fernandes F, Loura LMS, Chichón FJ, Carrascosa JL, Fedorov A, Prieto M. Biophys J. 2008; 94:3065. [PubMed: 18199667]
21. Bhatia VK, Madsen KL, Bolinger PY, Kunding A, Hedegard P, Gether U, Stamou D. EMBO J. 2009; 28:3303. [PubMed: 19816406]
22. Bhatia VK, Hatzakis NS, Stamou D. Semin Cell Dev Biol. 2010; 21:381. [PubMed: 20006726]
23. Madsen KL, Bhatia VK, Gether U, Stamou D. FEBS Lett. 2010; 584:1848. [PubMed: 20122931]
24. Hatzakis NS, Bhatia VK, Larsen J, Madsen KL, Bolinger P-Y, Kunding AH, Castillo J, Gether U, Hedegard P, Stamou D. Nat Chem Biol. 2009; 5:835. [PubMed: 19749743]
25. Doucet CM, Esmery N, de Saint-Jean M, Antonny B. PLoS ONE. 2015; 10:e0137965. [PubMed: 26366573]
26. Wimley WC, White SH. Nat Struct Mol Biol. 1996; 3:842.
27. Drozdetskiy A, Cole C, Procter J, Barton GJ. Nucleic Acids Res. 2015; 43:W389. [PubMed: 25883141]
28. Sen TZ, Jernigan RL, Garnier J, Kloczkowski A. Bioinformatics (Oxford England). 2005; 21:2787.
29. Farsad K, Ringstad N, Takei K, Floyd SR, Rose K, De Camilli P. J Cell Biol. 2001; 155:193. [PubMed: 11604418]
30. Ambroso MR, Hegde BG, Langen R. Proc Natl Acad Sci U S A. 2014; 111:6982. [PubMed: 24778241]
31. Chen Z, Shi Z, Baumgart T. Biophys J. 2015; 109:298. [PubMed: 26200865]
32. Shi Z, Baumgart T. Nat Commun. 2015; 6:5974. [PubMed: 25569184]
33. Jao CC, Hegde BG, Gallop JL, Hegde PB, McMahon HT, Haworth IS, Langen R. J Biol Chem. 2010; 285:20164. [PubMed: 20418375]
34. Poudel KR, Dong Y, Yu H, Su A, Ho T, Liu Y, Schulten K, Bai J. Mol Biol Cell. 2016; 27:2119. [PubMed: 27170174]
35. Zhu C, Das SL, Baumgart T. Biophys J. 2012; 102:1837. [PubMed: 22768939]

36. Ramesh P, Baroji YF, Reihani SNS, Stamou D, Oddershede LB, Bendix PM. Sci Rep-UK. 2013; 3:1565.
37. Prevost C, Zhao H, Manzi J, Lemichez E, Lappalainen P, Callan-Jones A, Bassereau P. Nat Commun. 2015; 6:8529. [PubMed: 26469246]
38. Yin Y, Arkhipov A, Schulten K. Structure. 2009; 17:882. [PubMed: 19523905]
39. Mim C, Cui HS, Gawronski-Salerno JA, Frost A, Lyman E, Voth GA, Unger VM. Cell. 2012; 149:137. [PubMed: 22464326]
40. Cui H, Mim C, Vázquez Francisco X, Lyman E, Unger Vinzenz M, Voth Gregory A. Biophys J. 2013; 104:404. [PubMed: 23442862]
41. Daum B, Auerswald A, Gruber T, Hause G, Balbach J, Kühlbrandt W, Meister A. J Struct Biol. 2016; 194:375. [PubMed: 27016283]
42. McMahon HT, Boucrot E. Nat Rev Mol Cell Biol. 2011; 12:517. [PubMed: 21779028]
43. Iversen TG, Skretting G, van Deurs B, Sandvig K. Proc Natl Acad Sci U S A. 2003; 100:5175. [PubMed: 12682302]
44. Capraro BR, Shi Z, Wu T, Chen Z, Dunn JM, Rhoades E, Baumgart T. J Biol Chem. 2013; 288:12533. [PubMed: 23482561]
45. MacDonald RC, MacDonald RI, Menco BPM, Takeshita K, Subbarao NK, Hu L-r. Biochim Biophys Acta Biomembr. 1991; 1061:297.
46. Diz-Munoz A, Fletcher DA, Weiner OD. Trends Cell Biol. 2013; 23:47. [PubMed: 23122885]
47. Tian A, Baumgart T. Biophys J. 2009; 96:2676. [PubMed: 19348750]
48. Sorre B, Callan-Jones A, Manzi J, Goud B, Prost J, Bassereau P, Roux A. Proc Natl Acad Sci U S A. 2012; 109:173. [PubMed: 22184226]
49. Capraro BR, Yoon Y, Cho W, Baumgart T. J Am Chem Soc. 2010; 132:1200. [PubMed: 20050657]

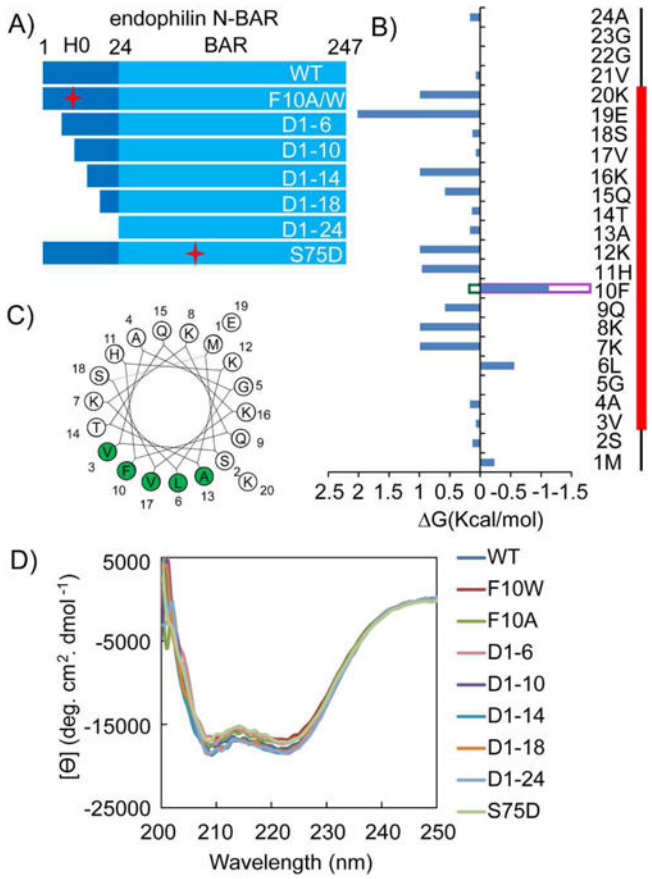

Figure 1. Membrane binding of endophilin N-BAR variants depends on molecular details of its amphipathic helices

A. Domain structure of endophilin N-BAR (WT) and H0 variants (single site mutagenesis: F10A, F10W; H0 truncation mutagenesis: D1-X indicates deletion of H0 residues from #1-#X), as well as H1i variant S75D. B. Residue hydrophobicity (from water to membrane surface)[26] of the H0 sequence and the predicted helix (red bar) by JPred 4[27] and GOR V[28]. Green and purple edged bars at #10 represent residues A and W respectively. C. Helical wheel projection of the H0 helix, where green-labeled residues indicate a hydrophobic surface. D. Circular dichroism spectra of endophilin N-BAR and its variants. All variants show helicity equivalent to the WT protein. Samples were tested in protein buffer (see materials and methods).

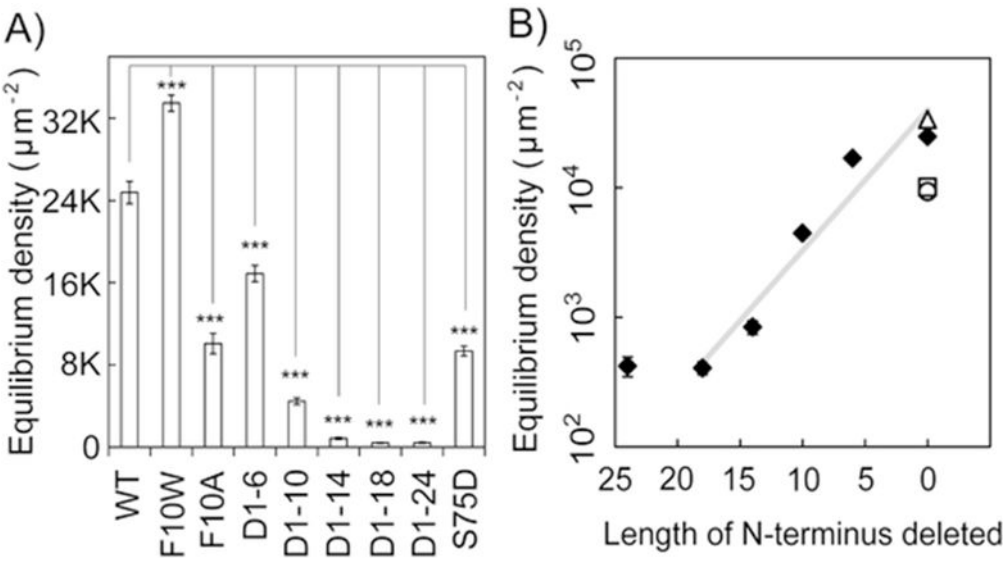

Figure 2. Amphipathic helices dominate the membrane binding of endophilin N-BAR

A. The equilibrium protein binding density (for 1 μM bulk concentrations) on GUVs: 24.5% DOPC/30% DOPE/45% DOPS/0.5% TexasRed -DHPE. At least five GUVs were measured and error bars are standard error of the mean. B. Logarithmic plot of equilibrium density vs. length of H0. Filled diamonds are data points of WT and truncation variants; open triangle, open square, and open circle refer to F10W, F10A, and S75D, respectively. Line is a guide to the eye.

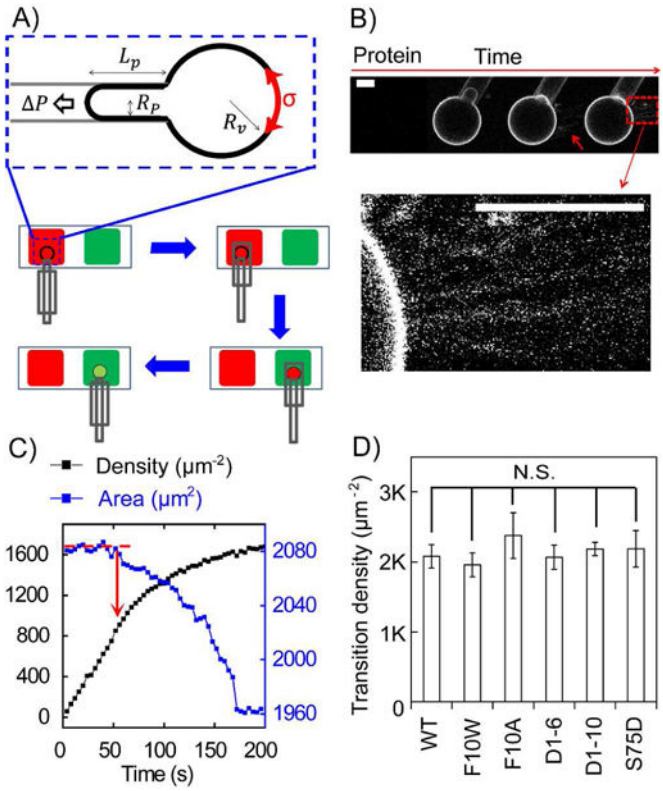

Figure 3. Intrinsic curvature generation capacity of endophilin N-BAR does not depend on amphipathic helices, as assessed by membrane shape stability assay

A. The geometry of glass-pipette aspirated GUV and the process of transferring a GUV from a GUV dispersion to protein solution. R_V: GUV radius; R_P: micropipette radius; L_P: projection length; ΔP: pressure difference). B. Time-lapsed confocal image of a transferred GUV in an N-BAR domain solution. Arrows indicate tubules formed towards the outside of the GUV. The image area contained in the dashed red box is also shown enlarged to zoom in on the formed tubules. Scale bar = 10 μm. C. Plot of protein density on GUV and the apparent area of the GUV (see Materials and Methods for the calculation). Red dashed line indicates that the apparent area was stable before the transition point (red arrow) when the area started to decrease. D. Comparison of transition densities of the variants at similar membrane tension of 0.040 ± 0.005 mN/m. At least five GUVs were counted for each protein and error bars are standard errors of the mean. GUV lipid composition: 24.5% DOPC/30% DOPE/45% DOPS/0.5% TexasRed -DHPE.

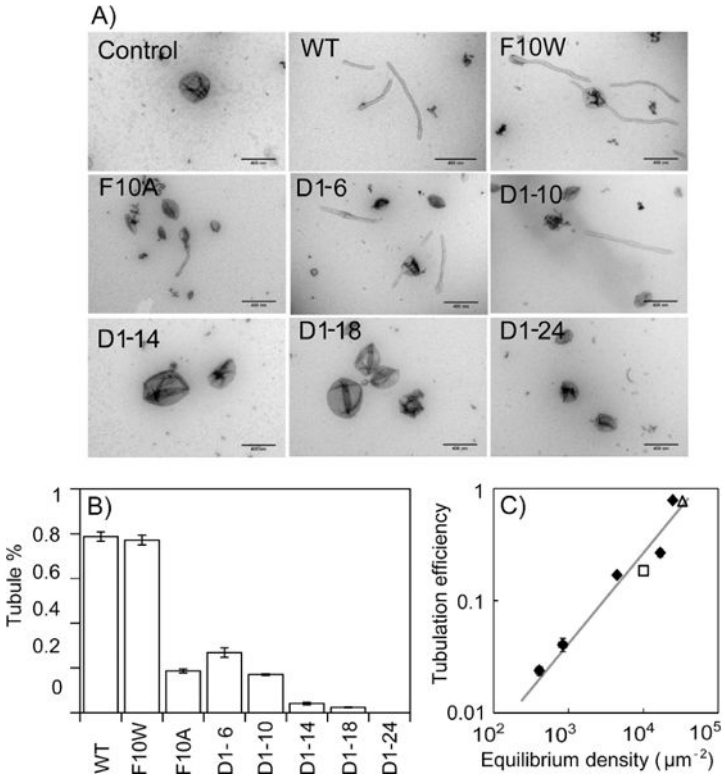

Figure 4. Overall tubulation capacity depends on membrane binding

For all variants, 0.1mg/ml LUVs were incubated with 10 μM proteins for 30 min in protein buffer. A. Representative TEM images of each variant. Scale bar = 400 nm. B. Quantitative tubulation percentage of LUVs. Tubule% = # of tubules/(# of tubules + # of LUVs). C. Logarithmic plot of tubulation efficiency vs. logarithmic plot of equilibrium density. Filled diamonds are data points of WT and truncation variants; open triangle and open square refer to F10W and F10A, respectively. The error bars are standard errors of the mean.

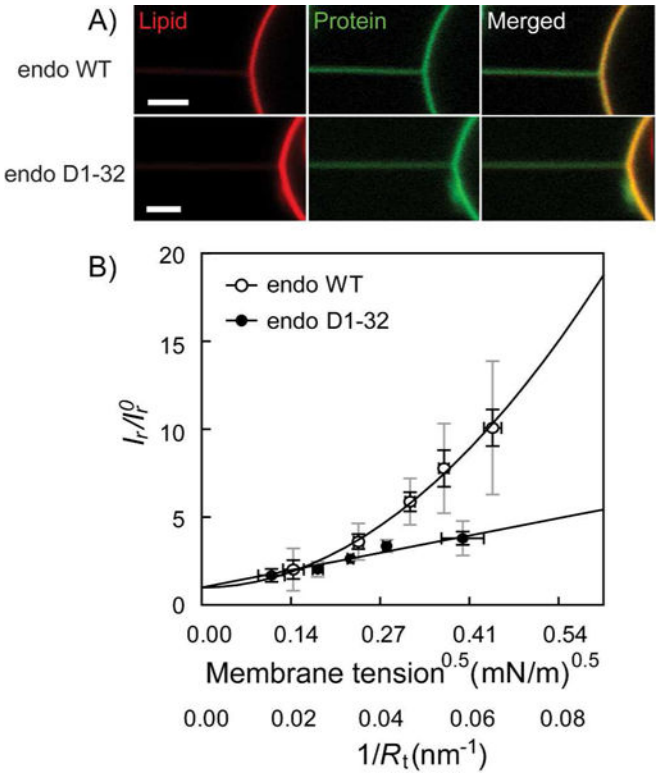

Figure 5. Both WT endophilin N-BAR and D1-32 mutant are sorted by membrane curvature

A. Confocal images of pulled tether-GUV system in the presence of WT endophilin N-BAR and D1-32 mutant. B. Relative fluorescence intensities (protein versus lipid) are compared on highly curved tether (I_r) and vesicle (I_r^0), tether radius (R_t) decreases with rising membrane tension. Experiments were done at the same protein membrane densities, while the bulk protein concentration for WT is 40 nM and for D1-32 is 154 nM. Grey and black error bars are standard deviation and standard error of the mean, respectively. GUVs: 64% DOPC, 25% DOPG, 10% PI(4,5)P2, 0.3% TexasRed DHPE and 0.7% DSPE-Bio-PEG2000. Membrane bending stiffness used for tether radius calculation is 23 K_BT[32].